Investigation of the effect of wrinkle features on wind turbine blade sub-structure strength

Bender, J. J.; Hallett, S. R.; Lindgaard, E.

Published in:
Composite Structures

DOI (link to publication from Publisher):
10.1016/j.compstruct.2019.03.026

Publication date:
2019

Document Version
Accepted author manuscript, peer reviewed version

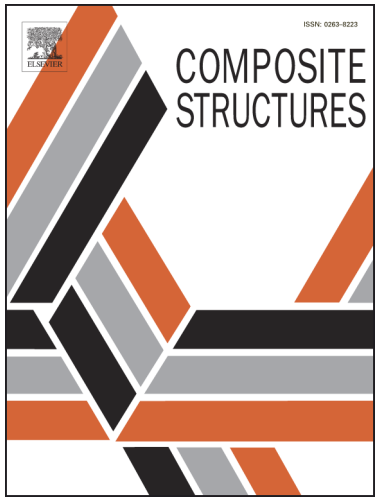

Investigation of the Effect of Wrinkle Features on Wind Turbine Blade Sub-structure Strength

J.J. Bender, S.R. Hallett, E. Lindgaard

PII: S0263-8223(18)33498-6
DOI: https://doi.org/10.1016/j.compstruct.2019.03.026
Reference: COST 10754

To appear in: *Composite Structures*

Received Date: 1 October 2018
Revised Date: 18 January 2019
Accepted Date: 6 March 2019

Please cite this article as: Bender, J.J., Hallett, S.R., Lindgaard, E., Investigation of the Effect of Wrinkle Features on Wind Turbine Blade Sub-structure Strength, *Composite Structures* (2019), doi: https://doi.org/10.1016/j.compstruct.2019.03.026

Investigation of the Effect of Wrinkle Features on Wind Turbine Blade Sub-structure Strength

J. J. Bender[1,*], S. R. Hallett[2] and E. Lindgaard[1]
[1]Department of Materials and Production, Aalborg University, Fibigerstraede 16, 9220 Aalborg East, Denmark
[2]Bristol Composites Institute (ACCIS), University of Bristol, Queens Building, Bristol BS8 1TR, United Kingdom
* Corresponding author email address: bender@mp.aau.dk

Abstract
Wrinkles are known to have a strong knock-down on the mechanical performance of structures made from composite materials. Here, static tensile tests were conducted to investigate the effect of wrinkle features on the strength of a wind turbine blade sub-structure, representative of a blade root feature. A pultruded tapered insert is embedded in each sub-structure and the wrinkle is in close vicinity to the termination of the tapered insert. Each of the tested sub-structures was then numerically modelled using finite element simulations. The numerical representations of the wrinkle geometries were constructed based on measurements of the actual structures, and an automatic fitting of the four chosen wrinkle features; angle, depth, wash out, and location. There is less than 5% deviation between the simulation and experimental results for all tested sub-structures. The numerical model was able to predict when the failure mode changed from a delamination at the tapered insert to a delamination in the wrinkle area. The average wrinkle angle was found to be a better metric than the maximum wrinkle angle to characterise the severity of the wrinkles in the vicinity of a tapered insert.

Keywords: *Sub-structure, Wrinkle defect, Tapered beam, Cohesive Zone*

1. Introduction

Wind Turbine Blades (WTBs) are getting larger and heavier each year, and to reduce the increase in weight of the WTBs it is necessary to make use of the full potential of the composite materials they are constructed from. The root experiences the highest loads in a WTB and therefore the most material is located in this area. If the materials are used more efficiently in this region, a significant reduction in weight can be achieved. A better understanding of the load conditions and the corresponding failures in the root section is required to reduce the amount of materials used, for which it is necessary to perform experiments. However, this poses a challenge since the root laminates are thick, and therefore standard coupon tests are not representative of the conditions in this region. Furthermore, full scale testing is complex and expensive, and so it is best avoided where possible. Therefore, component or sub-structure testing is a viable option to examine the behaviour and failure mechanisms in the root of WTBs.

A further complication is the risk of manufacturing defects, especially wrinkles, which are common in thick laminates [1–4]. Moreover, the transition from the thick root laminate to the thin laminates in the aerofoil section of the blade can also cause wrinkle defects. The effect of these wrinkle defects in the root section is not well documented. Therefore, it is highly relevant to determine the effect of different wrinkles on the strength of the root section of a WTB, in order to determine which wrinkles should be repaired e.g. using scarf patches [5], and which have a negligible effect, and therefore, can be left in the blade.

Recently, DNV-GL [6] modified the certification rules to include some sub-structure testing. The tests are related to structural adhesive bond lines and bonded inserts for bolted joints. Furthermore, sub-structure tests can be used instead of a full-scale test if the blade to be tested is similar to an already tested blade and the only difference is the area or structural detail which is tested through the sub-structure testing. Additionally, the sub-structure should be designed so that the boundaries do not affect the investigated area, and the load is representative of the blade load in the investigated area. The recent changes in the certification standard are partly due to research in the area [7–10]. Researchers are still working on maturing the field of sub-structure testing to be able to perform more sub-structure tests and less full-scale tests. Most of the work on sub-structures for WTBs is focused on the I-beam in the spar cap [7–9,11] because it is the primary load carrying component of the blade. Nevertheless, some research is focused on the aerodynamic shell [12], and some is focused on the trailing edge [10,13–15]

In [7] 4-point bending of an I-beam was conducted. The beam initially failed unintentionally by delamination at the load introduction points. After reinforcements in these areas, the failure occurred away from the loading areas. In [8] a combined I-beam and C-beam was designed. Precaution was taken to ensure failure away from the support and load introduction, which was achieved with a long slender beam. In [9] I-beams were tested in 4-point bending to evaluate the stress state in the bonded joint between spar caps and shear web. The 4-point bending resulted in damage evolution and final failure at the support locations. In [11] a C-beam was tested in asymmetrical 3-point bending. The aim was to test the bonded joint between the spar cap and the web of a WTB. The first failure of the C-beam occurred away from the support, and final failure occurred at the support due to delamination in the bonded joint between the spar cap and web. The final failure occurred close to the support, where the load was highest, but not representative of loads in a WTB.

In [12] a multiaxial test rig was developed to test the failure behaviour of grid-scored sandwich panels from the aerodynamic shell when a combination of bending and tension or compression was applied. The grid-scored foam core of the sandwich panel acted as a damage initiator, which ensured weak points that promoted failure away from the load introduction.

In [10] cut-outs of the trailing edge of an actual WTB were tested in a custom built test rig. The load case was similar to a blade in edgewise bending. It was reported that the boundaries of the sub-structure were weak points, meaning that failure initiated in these regions. It was emphasised that the central region should be made weaker or the boundaries should be reinforced to avoid failure at the boundaries, where the resulting failure load and mode were less representative of the actual failure load and mode.

In some cases wrinkles affect the surface plies causing a bulge [16–20] and in other cases the wrinkle is constrained within the laminate [4,21,22], in which the latter is similar to the current study. A few works dealing with wrinkles are described below where the wrinkle configurations are similar to the configurations in this work meaning wrinkles constrained in the laminate. In [22] a Glass Fibre Reinforced Polymer (GFRP) plate was manufactured with a wrinkle of 12° through the entire thickness. The resulting tensile strength reduction was ≈22%. In [23] a wrinkle of 29° was introduced in

a GFRP laminate, affecting half the thickness of the laminate. The resulting tensile strength reduction was 14%. In [21] a Carbon Fibre Reinforced Polymer (CFRP) plate was manufactured with a wrinkle in the central region. The wrinkle had an angle of 12°, and most of the plies through the thickness were affected to some extent. The resulting tensile strength reduction was ≈20%.

From the above sections it is clear that the load introduction locations are weak points when testing sub-structures, mostly because of the high stress concentrations. In this work, a tapered insert is terminated in the central region of the sub-structure, and a wrinkle is present in this region as well. Therefore, there are natural weak points away from the load introduction areas, meaning that the intended failure should not be affected by the load introduction.

This work is focused on experimentally quantifying the effect of a wrinkle defect in the vicinity of the termination of a tapered insert. In [24] it was determined that four features can be used to model a wrinkle and its shape through the thickness of a laminate. These features are the height of the wrinkle, the length of the wrinkle, the depth of effect or the number of affected plies, and the wash out degree, which is a measure for the height of the wrinkle through the thickness of the laminate. The location of the wrinkle w.r.t. the termination of the tapered beam is used as well but is special for the case where a tapered beam is included. The geometric features are used to construct a unique FE model for each manufactured sub-structure and numerical simulations are conducted to compare the predictive capabilities of the FE model with the experiments.

In Section 2 the manufacturing of the sub-structures and the test setup are described. In Section 3 the numerical models are presented, including the method to obtain the wrinkle features and the final FE models. In Section 4 the results are presented with a focus on the load-strain response and failure loads in experiments and simulations. The difference of wrinkles in flat laminates and near the tapered insert are discussed in Section 5. Finally, a conclusion of the work is presented in Section 6.

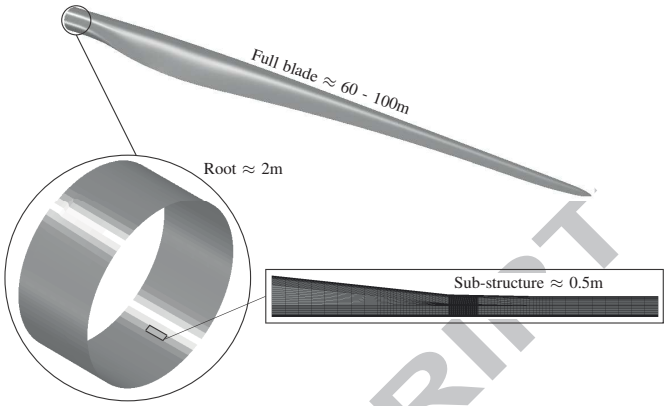

Fig. 1 Illustration of scales involved in testing Wind Turbine Blades.

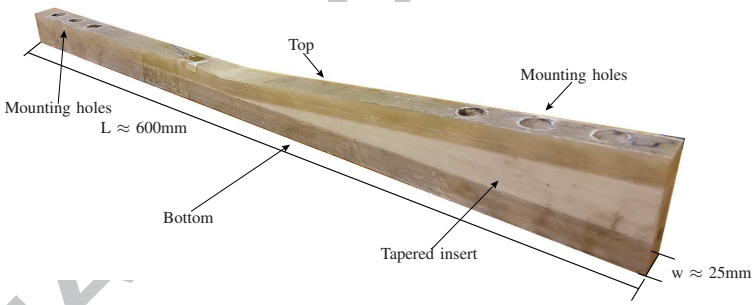

Fig. 2 Image of a manufactured sub-structure with approximate length, L, and width, w.

2. Experimental Setup

The sub-structures used in this work were manufactured to resemble the geometric shape and lay-up in the root section of a WTB, as indicated in Fig. 1. The indicated area of the root is at the transition from the root reinforcements to the regular spar laminate. This means that a pultruded beam with a taper was inserted in the centre of the sub-structure, as shown in Fig. 2. The sub-structures had a lay-up of biaxial fabric reinforcement (here labelled as BIAX) on the top and bottom surfaces, triaxial fabric (TRIAX) in the centre on either side of the insert, and unidirectional (UD) in the rest, as shown in Fig. 3. This lay-up is an exact copy of the laminate in a mass produced WTB. Therefore, the results are directly relatable to the strength of actual WTBs.

There is a factor of at least 100 in difference in size between the full blade and the sub-structure in Fig. 1, which indicates significant potential for savings in testing machinery and material costs.

The sub-structures in this work are loaded in tension. Compressive loading would be more critical for the wrinkle defect, however, tension loading is more severe for the tapered insert. An opening mode I stress is applied to the inclined surface of the tapered insert when tension loading is applied to the sub-structure. Therefore, tension loading is used to investigate the effect of the wrinkle on the most critical load condition of the tapered insert.

2.1 Sub-structure Manufacturing

Specimens with and without wrinkles were manufactured in the laboratory using the Vacuum Assisted Resin Transfer Moulding (VARTM) process. The wrinkles encountered in the root section of a WTB after manufacturing usually have a resin rich pocket close to the top of the laminate. In this work it was not possible to create an internal resin pocket without including either a pre-cured resin shape in the moulding of the laminate, or including fibres in the off-axis direction. In both cases the included artifact could have a significant influence on the result.

Instead, the wrinkle was introduced at the surface of the laminate, meaning that there was no resin pocket. Numerical simulations showed that a wrinkle at the surface caused final failure at a slightly lower load than a wrinkle starting in the laminate with a resin pocket. Therefore, it is assumed to be conservative to perform tests with surface wrinkles compared to more realistic internal wrinkles with a resin pocket. This is backed up by the findings in [25], where it is claimed that the resin pocket has almost no influence on the tensile results.

The wrinkles in this work were introduced in the laminate during the VARTM process. A wrinkle shape was used on top of the vacuum bag after the infusion, but before the resin was solidified as shown in Fig. 3. This manufacturing process is similar to the one described in [25], the primary difference is that they used the pressure from an autoclave to force the metal rod into the laminate, and in the present work, the force was applied manually. The force was applied to the wrinkle shape after the resin infusion was complete, until it was pressed half-way into the laminate. This ensured that the surface wrinkle had the desired dimensions and that the layers all the way to the tip of the insert were affected by the wrinkle. It was important that the indentation depth was controlled in order to avoid excess waviness of the layers below the insert since the bottom layers are not affected by the wrinkles found in actual blades. Two wrinkle shapes were used to manufacture the wrinkles. The first was a half-moon shape, which had a height of 4mm and a length of 20mm. The second shape was a round bar of 12mm in diameter. These two different shapes were used to achieve wrinkles with varying maximum wrinkle angles. The resulting wrinkles were characterised in the same manner as described in [24], which means that the

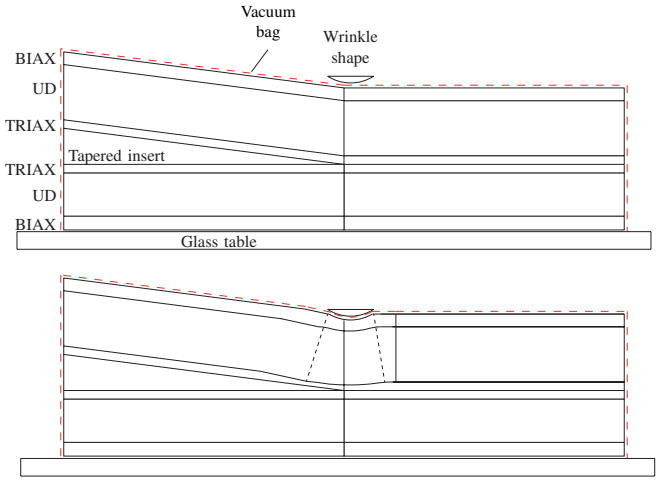

Fig. 3 Schematic of the manufacturing of the sub-structure with a wrinkle, before and after infusion. (The vacuum bag is indicated by red dashed lines.)

Table 1 This table lists the geometric parameters for the manufactured sub-structures. The wrinkles in sub-structures 3-5 are produced with the half-moon shape and the wrinkles in sub-structures 6-8 are produced with the round bar. The location is defined w.r.t. the tip of the insert, i.e. positive location means that the wrinkle is on the thin part of the sub-structure.

No.	Height (mm)	Length (mm)	Depth (mm)	Wash out (-)	Location (mm)	Maximum angle (°)
1	0	0	0	0	0	0
2	0	0	0	0	0	0
3	0.8	30	8.3	1.4	+4	5.0
4	1.1	35	16.2	1.4	+3	5.8
5	0.8	25	12.2	0.7	+2	5.9
6	1.0	17	17.9	0.7	+5	10.5
7	1.1	17	10.0	1.0	+5	11.8
8	1.2	17	11.9	0.7	+4	12.6

location, depth of effect, wash out degree, length, and height were defined for each wrinkle. These features are illustrated in Fig. 4. The length and height features are used to calculate the dependent maximum wrinkle angle, and the average wrinkle angle is calculated as in Eq. 1 [24].

$$\theta_{avg} = \frac{1}{t} \cdot \begin{cases} \int_0^t tan^{-1}\left(\frac{\pi \cdot a_y(y)}{L_y(y)}\right) dy & y \leq depth \\ 0 & y > depth \end{cases} \quad (1)$$

where

$$a_y(y) = a \cdot \left(1 - \left(\frac{y}{depth}\right)^w\right) \quad (2)$$

$$L_y(y) = L + y \quad (3)$$

where θ_{avg} is the average wrinkle angle, t is the thickness from the top of the laminate to the tip of the tapered insert, y is the distance in the through-thickness direction from the top surface of the sub-structure to an arbitrary point between the top surface and tip of the insert, a_y is the height of the wrinkle at a depth of y, $depth$ is the depth of effect of the wrinkle, w is the wash out degree, and L is the length of the wrinkle.

The resulting features of the wrinkles in the manufactured sub-structures are listed in Table 1. The table shows that two pristine sub-structures were tested, namely sub-structure 1 and 2, three sub-structures manufactured with the half moon namely sub-structure 3-5, and three sub-structures manufactured with the round bar namely sub-structure 6-8. The table also shows that there is a significant difference in the maximum wrinkle angle from the wrinkles made with the half-moon and the round bar.

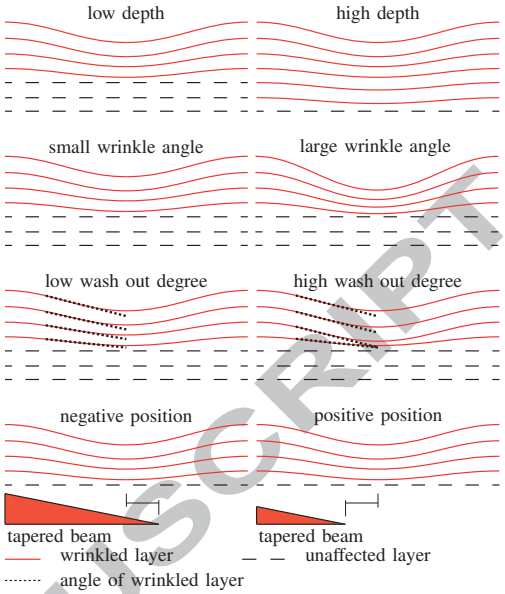

Fig. 4 Illustrations of how the four features affect the wrinkle shape through the thickness of the model. The red solid lines indicate the layers affected by the wrinkle, the black dashed lines indicate the unaffected straight layers, and the black dotted lines indicate the wrinkle angle of the separate layers to show the effect of the wash out degree. [24]

2.2 Test Setup

The test setup is shown in Fig. 5 with a sketch of the fixture. The static tensile tests were performed in a 400kN test machine, and the load throughout the tests were recorded through a load cell of similar capacity. A high speed camera was used to capture the damage evolution at the point of delamination. The camera was triggered manually at the unmistakeable sound of the delamination. Strain gauges were attached on the top and bottom side of the sub-structures ≈60mm away from the tip of the insert to ensure that the geometrical changes from the insert and the wrinkle did not directly affect the strain results. The displacement was continuously increased during the test until delamination where the load was reduced to zero. The fixtures as shown in the sketch in Fig. 5 were designed with adjustment screws to accommodate sub-structures with slightly varying thicknesses. By adjusting the screws, the centre of the load introduction could be aligned with the centre of the sub-structure to ensure accurate tensile loading.

The adjustment screws could also be used to introduce an eccentricity to the load condition and hereby introduce a moment loading as well. This was not utilised in this work. When the load is introduced in the centre of the sub-structure there is no rotation in the bottom grip in the thin end due to friction in the joint (Fig. 5). However, a small amount of rotation occurs in the top around the y-axis, which is accounted for in the modelling.

3. Numerical Models

The numerical FE model used in this work was developed as part of the work in [24], and therefore, thoroughly described therein. However, a brief overview of the main points of the FE model is included in the following. The FE model is made in ABAQUS 2016 and solved using the explicit solver, with the actual densities of the materials and no mass scaling. The model is shown in Fig. 6 and has one solid element, of the type C3D8R, in the width direction making it a slice model. The mesh in the x-direction is increased in density closer to the tip of the insert and the wrinkle. The element lengths are determined based on convergence studies and the largest

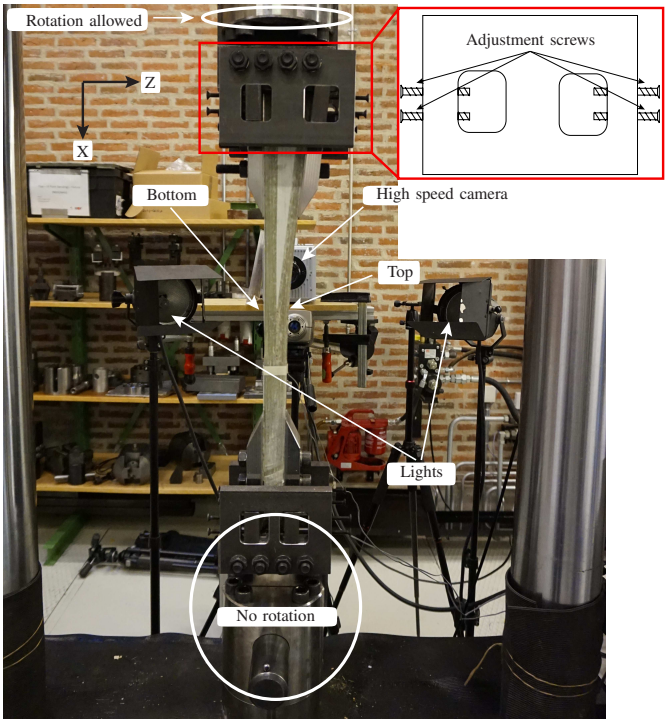

Fig. 5 The test setup is comprised of a high speed camera, lights to allow a high frame rate, and strain gauges on the top and bottom surfaces of the sub-structure.

elements are 10mm long and the shortest are 1mm. It is constrained on one surface in the width direction allowing the nodes on the other surface to contract freely during loading, which yields a plane stress condition. Cohesive elements,of the type COH3D8, are inserted in the interfaces between all the layers in the model, which yields a total number of degrees of freedom of 63054. The built-in ABAQUS material model for the cohesive elements was used in the simulations with a bilinear softening law and mode mixity was accounted for through the Benzeggagh-Kenane criterion. The material data used in the models was provided by the manufacturer of the sub-structures. However, the actual values can not be disclosed. The onset traction values in mode I and mode II for the cohesive law were fitted based on a pilot tension test of a sub-structure cut out from a real blade. The onset tractions were fitted so that the load at insert delamination was similar for the experiments and the simulations. Furthermore, the onset tractions were physically feasible after the fitting and their mutual relation was acceptable. All other material parameters were used as supplied by the manufacturer.

The loading is applied as a prescribed displacement on the entire cross-sectional area at the end of the thin part of the sub-structure. This means that no rotation can occur in the thin end of the sub-structure. Since the sub-structure is tapered on one surface there is no symmetry line, and therefore no straight centre line. The centre line has one end point at the centre of the height in the thin end and one in the centre of the height in the thick end. Displacement in the length-direction is constrained in the thick end at a height corresponding to the centre of the height in the thin end, which means that rotation can occur in this end. This is chosen because the sub-structures are loaded in both ends at a height corresponding to the centre of the thin end in the experiments.

Complete control of the final wrinkle geometry in the physical specimens is almost impossible. Therefore, the laminates were manufactured, and afterwards, the corresponding numerical models were constructed, based on images of the manufactured sub-structures

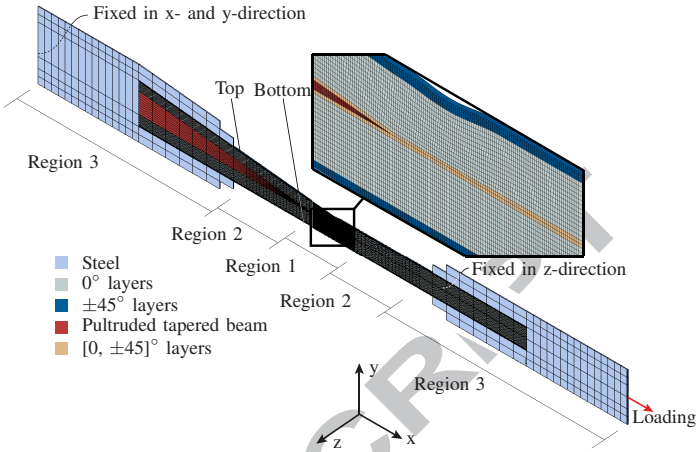

Fig. 6 Mesh of the FE model with a close-up at the wrinkle and tip of the tapered beam. [24]

and fitting of the four features. The images were captured with a microscope set to x0.63 magnification, and a light source was placed on the back side of the sub-structure to transilluminate it. A unique FE model was constructed for each manufactured sub-structure since all the wrinkles were slightly different. The BIAX layers on the top were easily detectable in the image due to the darker color. The stitching in the UD plies was detectable as well in some of the plies. These contours were used to determine the correct heights, lengths, depths, wash out degrees, and locations of the wrinkles in the sub-structures.

The depth, height, and wash out degree were determined by

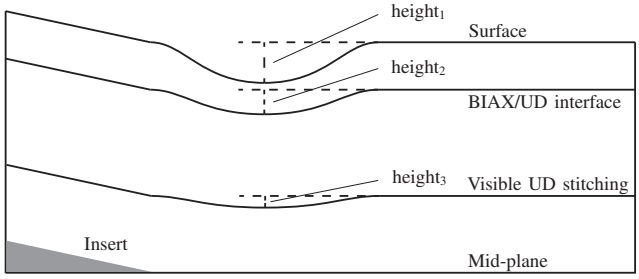

Fig. 7 Illustration of the fitting process.

measuring the height of the wrinkle at discrete points through the thickness as shown in Fig. 7. With these 3 height values, or misalignment values from the original straight line, it was possible to determine the depth, height, and wash-out degree. In this work, this was done by an automatic fitting in MATLAB using the ”fminunc” function. All the combinations of wrinkle height, depth, and wash out degree produce different height values through the thickness. The ”fminunc” optimises the parameters to minimise the square of the error between the measured 3 height values and the resulting simulated heights from the combination of height, depth, and wash out degree.

The problem has multiple local minima, so the fitting is started at multiple initial conditions to increase the probability that a global minimum is achieved. Afterwards the three fitted parameters are used as input in the numerical model. The interface lines from the resulting geometrical models are overlaid on the images of the sub-structures, as in Fig. 8 and 9. The length and location of the wrinkle are manually fitted based on these combined images until a satisfactory agreement is achieved between the location of the tip of the insert compared to the wrinkle and the slope of the wrinkle. The final fit for a sub-structure where the wrinkle is produced with the half-moon and the round bar is shown in Fig. 8 and Fig. 9,

respectively.

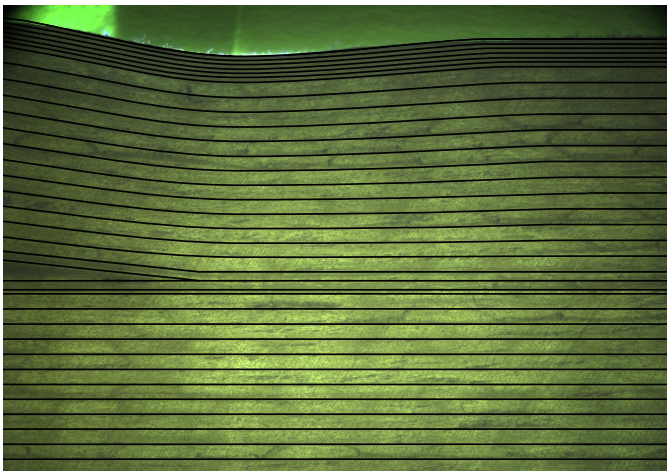

Fig. 8 Fitting the numerical wrinkle to the wrinkle produced with the half-moon in the manufactured laminate. (The black lines indicate the cohesive interface elements)

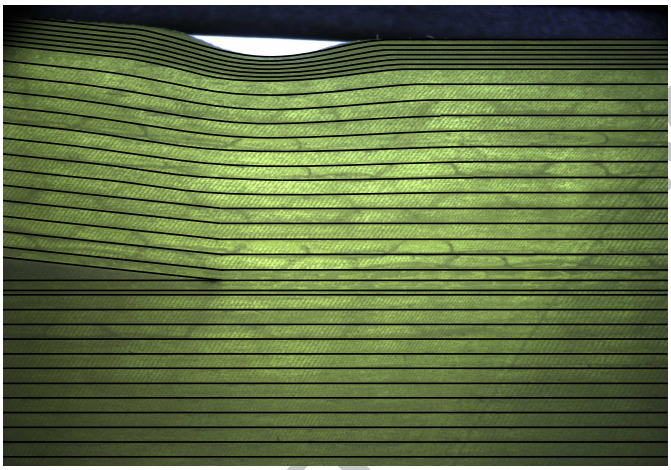

Fig. 9 Fitting the numerical wrinkle to the wrinkle produced with the round bar in the manufactured laminate. (The black lines indicate the cohesive interface elements)

4. Results

Static tensile tests of manufactured WTB sub-structures were conducted. Load-strain data was recorded during testing and high speed images were captured during the delamination failure. Two pristine sub-structures without wrinkles and six sub-structures with wrinkles were tested. The mean load-strain curves of all the tested sub-structures are shown in Fig. 10 along with the standard deviation. It is shown that the load and strain increases monotonically throughout the test until final failure.

The relatively small variation in Fig. 10 shows that the load as a function of strain in the length direction is similar for all the tested sub-structures. The solid green line indicates the mean value of the strain on the top side of the sub-structures and the solid red line indicates the mean value of strain on the bottom side of the sub-structures. The shaded areas are the standard deviation, and the dashed lines show the load-strain curves for a simulation of a pristine sub-structure. There is a fairly good agreement between the strain in the experiments and the strain in the simulation. The bending of the sub-structure is proportional to the difference in strain on the top and bottom of the sub-structure. Based on the data there is no correlation between the amount of bending and the load at final failure. Nor is there any relation between the severity of the wrinkle and the bending in the sub-structure.

Images from the high speed camera are shown in Fig. 11. The

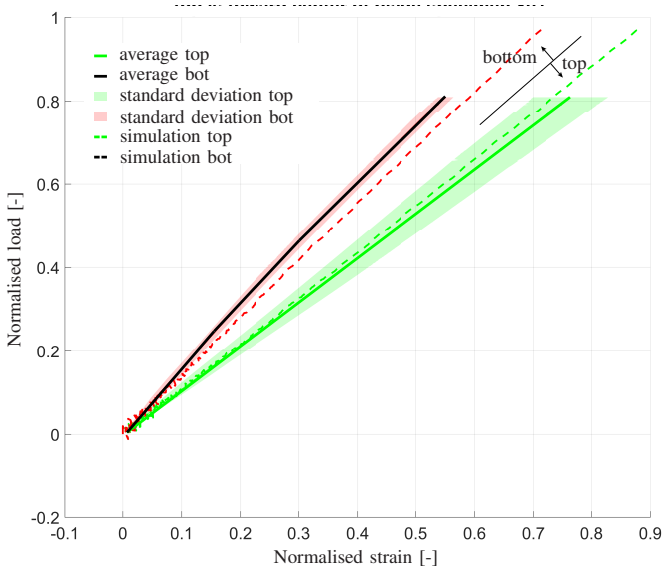

Fig. 10 The normalised load and strain on top and bottom for all the conducted experiments. The strain on top and bottom are averaged at each load point and indicated by the solid lines, the standard deviation is calculated as well and indicated by the shaded areas. The load-strain response of a simulation of a pristine laminate is shown as well as the dashed lines.

initiation point for the delamination at the tapered insert is indicated with a white circle, except for sub-structure 2 where the initiation happened outside the frame. For all the other sub-structures, the delamination at the tapered insert initiated at the tip of the insert. For the pristine sub-structures 1-2 only one frame is shown at full opening, and two frames are shown for the wrinkled sub-structures. One frame shows the sub-structure right before delamination at the wrinkle, and one frame shows the sub-structure at wrinkle delamination. All the sub-structures delaminated on the top and bottom of the insert, and on the thin side of the laminate as well. Delamination occurred at the insert first and then at the wrinkle for all wrinkled sub-structures except number 7, where the order was reversed. The special behaviour of sub-structure 7 was duplicated numerically through a numerical model where the width was increased, as described in more detail in the next section. The time from initiation of the insert delamination until complete delamination was less than 1ms.

The damage progression is as shown schematically in Fig. 12 for most of the sub-structures. A crack initiated at the tip of the insert and then simultaneously propagated in the direction of the thin and thick laminate on the top of the insert. A crack on the bottom of the insert initiated when the crack on the top started to open. Finally a crack initiated and opened in the wrinkle area. This behaviour is documented for the simulations through Fig. 13 where it is shown for a typical slice model that the damage index at the tip of the insert increases slowly, and damage occurs instantly at the wrinkle closely after complete damage at the insert. For the wide 3D model for sub-structure 7 it is shown that damage reaches a level of 1 at the wrinkle before the tip.

The maximum and average wrinkle angles for each of the tested sub-structures are shown in Table 2 along with the simulation and experimental knock-down and the error between the two for each sub-structure. The knock-down for the simulations are based on the

Fig. 11 High speed camera results. The upper image for all sub-structures shows the damage state after insert delamination except for sub-structure 7, and the lower image shows the damage state after wrinkle delamination except for sub-structure 1, 2, and, 7. The white circles indicate the delamination initiation point, the white arrow in sub-structure 2 indicates that initiation was outside the frame.

load at final failure from the simulation of the pristine sub-structure. The knock-down for the experiments is based on the average of the load at final failure of the tested pristine sub-structures 1-2. The minimum and maximum experimental values are 4.1% below and above the average, respectively, and therefore there is an 8% variation between the load at final delamination for these two sub-structures. One of the reasons for this can be found in the high-speed images where it is clear that the delamination for sub-structure 2 started on the thick part of the sub-structure at least 50mm away from the tip of the insert. Subsequently, this shows that there was a material flaw somewhere in the interface between the insert and the laminate that triggered failure earlier than at the insert, where the stress was highest. There could also be flaws in the other sub-structures, which could influence the results, meaning that the different wrinkle severities are not necessarily the only differences between the sub-structures.

The load at failure for the simulation is determined as the highest load before the load drop as indicated in Fig. 14. The load drop is distinct when the insert delaminates from the rest. For the wide 3D model of sub-structure 7 it is shown that there is a minor load drop when the delamination at the wrinkle initiates, but the major drop occurs later when the insert delaminates from the rest.

There is a good agreement between the knock-down in the simulations and the experiments as indicated by the errors in the last column in Table 2. Furthermore, the knock-down of the wrinkled sub-structures is more than 10% for most of the sub-structures, meaning that there is a difference between the strength of the pristine sub-structures and the wrinkled ones. The minimum and maximum of the experimental load at final failure for the pristine sub-structures was 4.1% in either direction of the average, indicating that the wrinkle knock-downs are outside of the experimental scatter. This is also shown in Fig. 15 and 16 where the results from Table 2 are illustrated.

Table 2 This table lists the maximum and average wrinkle angles along with the numerical and experimental strength knock-down for all the tested sub-structures. The wrinkles in sub-structures 3-5 are produced with the half-moon shape and the wrinkles in sub-structures 6-8 are produced with the round bar. The load values are normalised w.r.t. the width of the sub-structures, and the load at delamination for the pristine laminate for simulation and experiments, respectively. The "Error, sim exp"-column shows the difference between the failure loads in the simulations and experiments. The simulation results marked with an * are based on a full 3D model.

No.	Maximum angle (°)	Average angle (°)	Simulation knock-down (%)	Experimental knock-down (%)	Error, sim exp (%)
1-2	0	0	0.0	0.0	5
3	5.0	1.5	9.6	0.4	4
4	5.8	3.3	19.4	15.2	0
5	5.9	1.8	12.6	10.3	3
6	10.5	4.1	18.8	14.2	0
7	11.8	3.6	4.0*	-0.6	3*
8	12.6	3.7	19.5	14.1	1

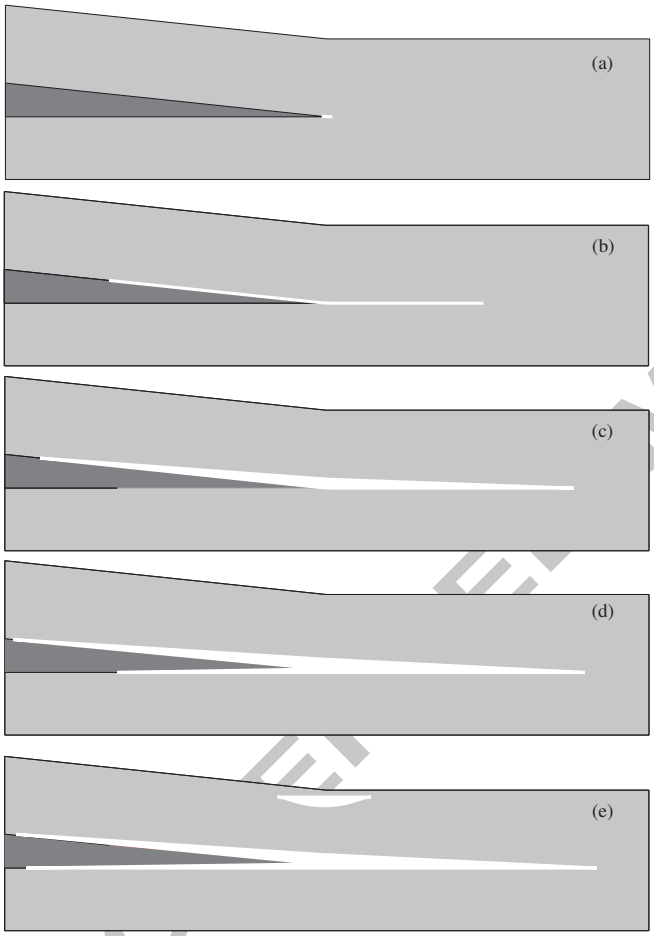

Fig. 12 Illustration of the damage propagation in most of the tested sub-structures. (a) initiation at the tip of the insert, (b) crack propagation on top of insert, (c) crack opening on top and crack propagation on bottom of insert, (d) crack opening on top and bottom of insert, (e) wrinkle initiation, propagation, and opening.

In Table 2 the maximum and average wrinkle angles indicate similar severity for most of the wrinkles, meaning that either parameter could be used to indicate the severity of the wrinkle. However, sub-structure 4 has a low maximum wrinkle angle but a relatively high average wrinkle angle, and in this case only the average wrinkle angle provides an accurate measure of the severity of the wrinkle. This is also graphically shown in Fig. 15 and 16 where the results from sub-structure 4 (indicated by the black ellipses) look like outliers when considering the maximum wrinkle angle in Fig. 15, but for the average wrinkle angle in Fig. 16 the data is in agreement with data points from the other experiments.

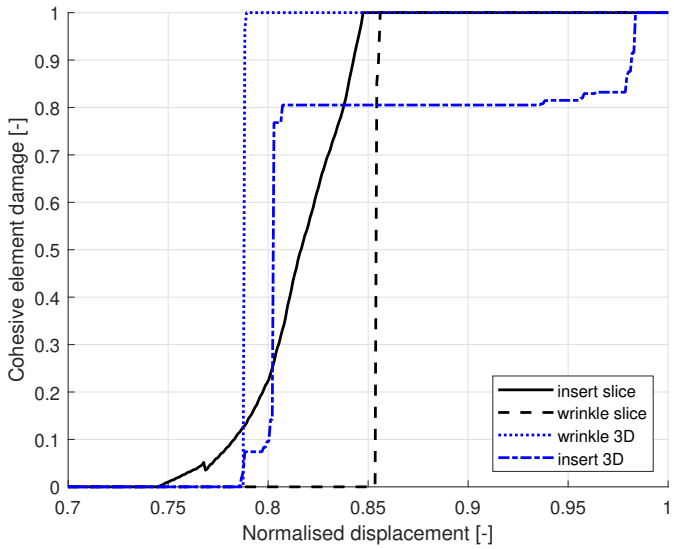

Fig. 13 Progression of damage index in sub-structure 7 for the slice and the 3D model. The damage index is extracted at the tip of the insert and at the ply where wrinkle delamination occurs in each of the models.

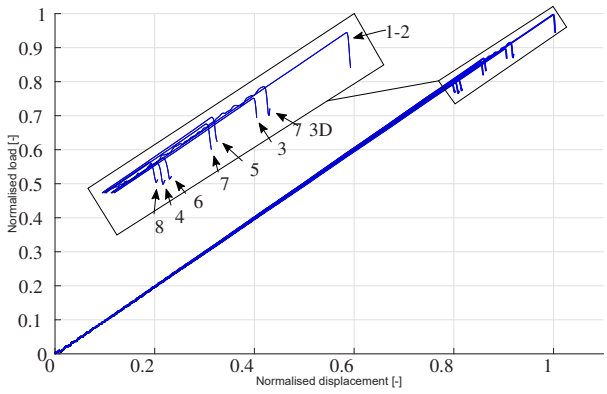

Fig. 14 The normalised load and displacement for each simulation. Each simulation result curve is identified with the corresponding sub-structure number. The result for sub-structure 7 is presented twice, once for a slice model and once for a 3D model.

5. Discussion

Sub-structure 3 does not exhibit a good agreement between the simulation and experiments with an difference in knock-down of 9%. There is nothing in the data that provides a clue as to why the difference is much higher than the rest. Furthermore, the knock-down from this experiment does not follow the trend from the rest of the experiments or simulations. In the experiments, the damage progression was different for sub-structure 7 than for the

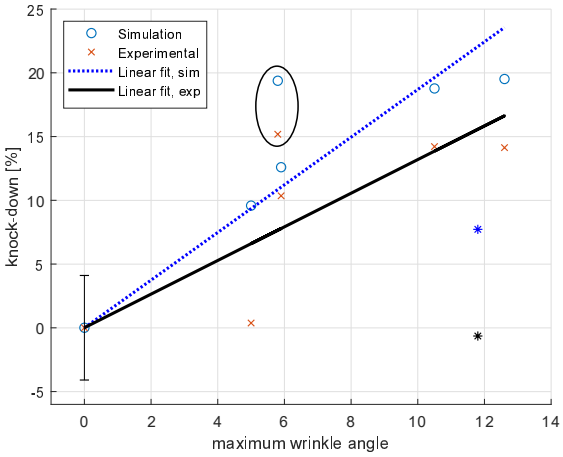

Fig. 15 Knock-down compared to the pristine laminate as a function of the maximum wrinkle angle. (The ellipse indicates the data from sub-structure 4, and the asterisks represent the data from sub-structure 7, which are considered outliers)

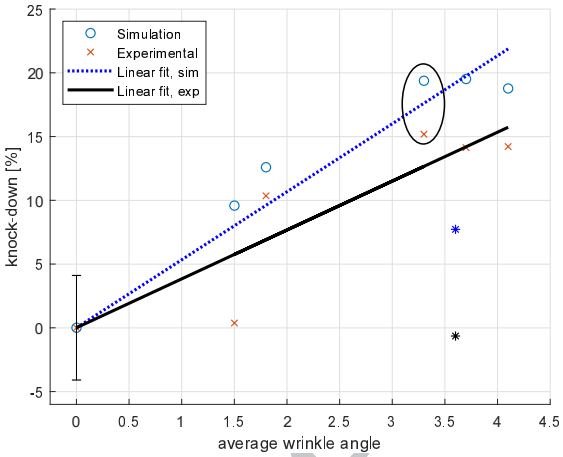

Fig. 16 Knock-down compared to the pristine laminate as a function of the average wrinkle angle. (The ellipse indicates the data from sub-structure 4, and the asterisks represent the data from sub-structure 7, which are considered outliers)

rest of the wrinkled sub-structures. A wrinkle delamination occurred at a load of 87% of the load for insert delamination. This damage progression is shown in Fig. 17. The behaviour was only captured in the simulation when a wide 3D model of 15 elements in the width direction was used instead of the slice model.This wide 3D model had a total number of degrees of freedom 498576.

The model was created by extruding the slice model in the width direction. The reason for using a wide 3D model in this work is that when the width of the model and boundary conditions are changed, the full free edge stress in properly captured, as shown in Fig. 18a and 18b. In Fig. 18a it is shown that the interlaminar normal stress at the wrinkle is increased by 30% at the edges compared to the slice model and the interlaminar shear stress is decreased 18%. It should be noted that the interlaminar normal stress is 10 times higher than the interlaminar shear stress at the wrinkle where this data is extracted. However, at the tip of the insert (Fig. 18b) the interlaminar normal stress is decreased at the edges, and increased close to the centre by 8%. These changes in stresses cause failure at the wrinkle to be more probable due to the increased stress. The change from a slice model to a wide 3D model has an insignificant effect for the sub-structures where the propagation of damage is unchanged. Meaning that if a delamination occurs first at the insert for the slice and wide 3D model, there is almost no difference in predicted strength. However, if the failure progression changes there can be a significant change in the predicted strength of the sub-structure. For example if the slice model predicts insert failure but the wide 3D model predicts wrinkle delamination followed by insert delamination.

The load at wrinkle delamination is predicted at 8% lower load than the wrinkle delamination in the experiment. Furthermore, the location of the wrinkle delamination is predicted with reasonable accuracy, as shown in Fig. 17. However, the predicted and actual knock-down of sub-structure 7 does not agree with the trend of the other tests w.r.t. the average wrinkle angle. This is to be expected because the failure mechanism for sub-structure 7 is different than the rest. Therefore, it would be unlikely that the trend would be similar for both failure mechanisms. For the other simulations it was not necessary to expand the slice model as similar results were obtained compared to a full 3D model.

As mentioned, the knock-down of a 12° wrinkle affecting the entire thickness of a flat laminate was reported to be around 20% for GFRP and CFRP in [22] and [21], respectively. In [23] the knock-down was 14% for a larger wrinkle of 29°, but only affecting half the thickness. From this and the findings in [24,26] it can be concluded that the number of affected plies, or the ratio of thickness affected by the wrinkle significantly affects the strength knock-down.

In this work the largest maximum wrinkle angle was 12.6° which is similar to the wrinkles reported in [21,22] and it was affecting almost half the thickness of the laminate, which is similar to the wrinkles in [23]. Based solely on this, a 12° wrinkle affecting half the thickness should yield a knock-down significantly below 14%. However, the knock-down for this particular wrinkle configuration was 14.1% in the experiments and 19.5% in the simulation. This means that wrinkles in the vicinity of the termination of a tapered beam, are more severe than wrinkles in flat laminates. A reason for this is increased interlaminar normal stress at the tip of the insert caused by the wrinkle. This is described in further detail in the following.

The simulated stress at the tip of the insert for three different sub-structures, namely 1, 5, and 7, are shown in Fig. 19. The stress is normalised w.r.t. the maximum shear stress of sub-structure 1 and the displacement is normalised w.r.t. the displacement at full failure (zero stress) for sub-structure 1. The out-of-plane shear and normal stress for the pristine sub-structure 1 are indicated by the solid lines in Fig. 19. The shear stress is higher than the normal stress, and both stresses increase until damage is initiated in one cohesive element at the tip and the shear stress starts to decline. When the damage of an element reaches 1 both stress components reduces to zero. The same trend is shown for the wrinkled sub-structure 5 but the normal stress is significantly higher compared to the pristine sub-structure 1. This means that the wrinkle significantly increases the normal stress at the insert and slightly increases the shear stress. This results in failure at a lower prescribed displacement.

The trend is different for sub-structure 7. The stresses increase until delamination at the wrinkle, which occurs at a normalised displacement of ≈0.75. The interlaminar stress at the tip decreases at this time but does not go to zero. The interlaminar normal stress in sub-structure 7 after the wrinkle delamination is only slightly higher than the interlaminar normal stress in the pristine sub-structure 1, which is why the final delamination occurs at a displacement and load similar to the ones for the pristine sub-structure 1.

It is shown in this work that the maximum wrinkle angle is not always the best metric for wrinkle severity. There is no doubt that it plays an important role in reducing the strength of a laminate, but as discussed, the depth and wash out degree are also important.

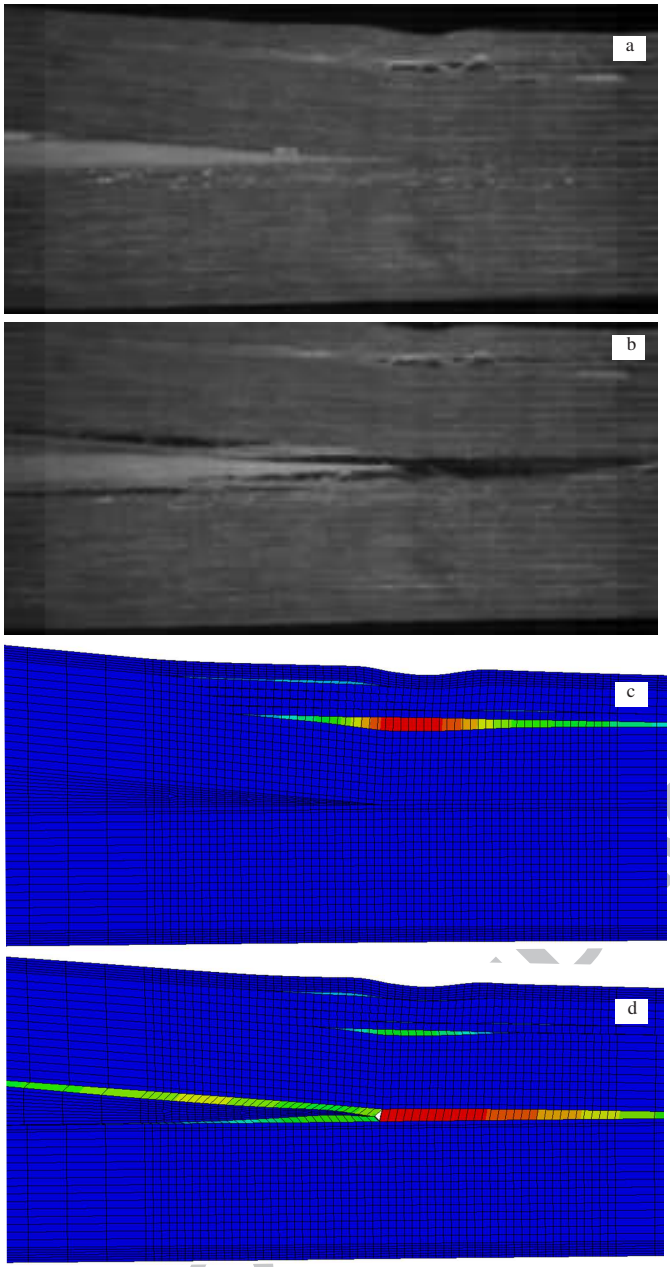

Fig. 17 High speed images of sub-structure 7 (a) before and (b) after insert delamination. Simulation results from a full 3D model (c) before and (d) after insert delamination for comparison. The color scale in (c,d) indicates the mode I opening displacement where red is highest.

From the experimental data in this work it seems that the average wrinkle angle is an appropriate measure for the wrinkle severity, which takes into account the wrinkle angle, depth, and wash-out degree. However, as noted in [24] the average wrinkle angle is only an appropriate measure when the average wrinkle angle is below 6° for the simulated and tested type of laminates. Above this threshold there is an increased probability that the final failure will be a delamination at the wrinkle instead of the tapered insert, and this change of damage mechanism can not be correctly identified through the average wrinkle angle alone.

6. Conclusion

An experimental and numerical investigation of the effect on tensile strength of wrinkle defects close to the tip of a tapered pultruded insert has been conducted. Overall a good agreement was found between the experimental and numerical results, which means deviations of less than 5%. The following conclusions have been drawn based on the conducted work:

- The semi-automatic determination of the wrinkle features proved stable and ensured good agreement between experimental and numerical results. Furthermore, the four identified features were sufficient to model all the manufactured wrinkles to a satisfactory level.
- The average wrinkle angle was a reliable metric for predicting the severity of the wrinkles and hence the knock-down of the tensile strength. This might not have been the case if the wrinkles had been more severe.
- The wrinkle defects increase the stress level at the tip of the pultruded insert, which means that compared to wrinkles of similar severity in flat laminates as found in the literature, significantly higher knock-downs occur when wrinkles are placed in the vicinity of the termination of a tapered beam.

From this work it is clear that the failure mechanisms related to wrinkles in the vicinity of the termination of tapered beams can be predicted by simulation tools with acceptable accuracy for static cases. However, fatigue is often a design driver for WTBs and other composite structures. Therefore, the fatigue behaviour of the sub-structures tested in this work should be studied in the future.

Acknowledgement

This work is part of a Ph.D. project at the Department of Materials and Production at Aalborg University, Denmark. The work is supported by the Innovation Fund Denmark project OPTI_MADE_BLADE, Grant No. 75-2014-3. This support is gratefully acknowledged.

References

[1] H. M. Hsiao and I. M. Daniel, "Elastic properties of composites with fiber waviness," *Composites Part A: Applied Science and Manufacturing*, vol. 27, no. 10, pp. 931–940, 1996.
[2] H. Hsiao and I. Daniel, "Effect of fiber waviness on stiffness and strength reduction of unidirectional composites under compressive loading," *Composites Science and Technology*, vol. 56, no. 5, pp. 581–593, 1996.
[3] H. J. Chun, J. Y. Shin, and I. M. Daniel, "Effects of material and geometric nonlinearities on the tensile and compressive behavior of composite materials with fiber waviness," *Composites Science and Technology*, vol. 61, no. 1, pp. 125–134, 2001.
[4] A. Makeev, G. Seon, E. Lee, B. H. Textron, and F. Worth, "Failure predictions for Carbon/Epoxy tape laminates with wavy plies," *Journal of Composite Materials*, vol. 44, no. 1, pp. 95–112, 2010.
[5] K. B. Katnam, A. J. Comer, D. Roy, L. F. M. Da Silva, and T. M. Young, "Composite repair in wind turbine blades: An overview," *Journal of Adhesion*, vol. 91, pp. 113–139, 2015.
[6] DNV-GL, "DNVGL-ST-0376 Rotor blades for wind turbines," Tech. Rep. December, 2015.
[7] J. F. Mandell, D. W. Combs, and D. D. Samborsky, "Fatigue of Fiberglass Beam Substructures," in *The Fourteenth ASME Wind Energy Symposium*, 1995, pp. 99–106.
[8] F. Sayer, N. Post, A. V. Wingerde, H. G. Busmann, F. Kleiner, W. Fleischmann, and M. Gansow, "Testing of Adhesive Joints in the Wind Industry," in *European Wind Energy Conference and Exhibition*, 2009, pp. 1–10.
[9] D. Zarouchas, A. Makris, F. Sayer, D. Van Hemelrijck, and A. Van Wingerde, "Investigations on the mechanical behavior of a wind rotor blade subcomponent," *Composites Part B: Engineering*, vol. 43, no. 2, pp. 647–654, mar 2012.
[10] M. A. Eder, K. Branner, P. Berring, F. Belloni, H. Stensgaard Toft, J. D. Sørensen, A. Corre, T. Lindby, A. Quispitupa, and T. K. Petersen, "Experimental Blade Research - phase 2," DTU Wind Energy, Tech. Rep., 2015.
[11] G. Fernandez, H. Usabiaga, and D. Vandepitte, "Subcomponent development for sandwich composite wind turbine blade bonded joints analysis," *Composite Structures*, vol. 180, pp. 41–62, nov 2017.

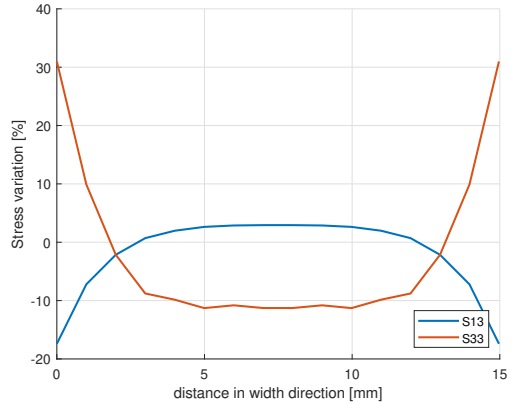

Fig. 18a Percent stress variation from slice to full 3D model at the wrinkle w.r.t. the width of the wide model

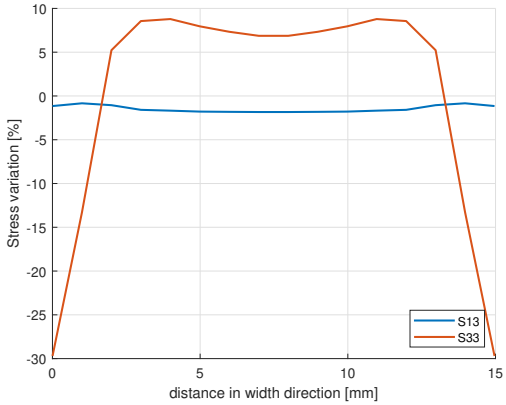

Fig. 18b Percent stress variation from slice to full 3D model at the tip of the insert w.r.t. the width of the wide model

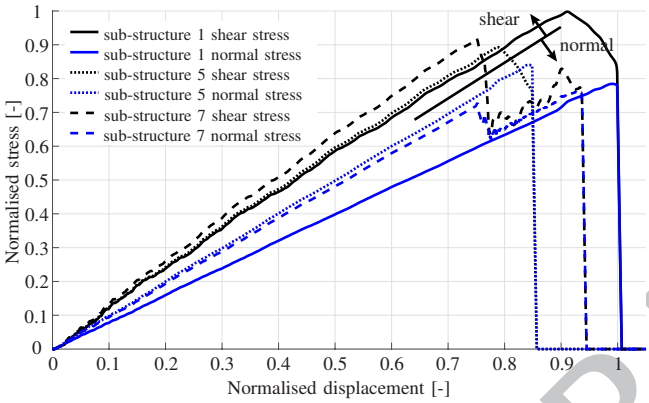

Fig. 19 Simulated out-of-plane normal and shear stress at the tip of the insert for sub-structure 1, 5, and 7. The data is filtered to remove high frequency numerical noise. The stresses are normalised w.r.t. the maximum shear stress, and the displacements are normalised w.r.t. the displacement when the stress drops to zero for sub-structure 1.

[12] S. Laustsen, E. Lund, L. Kühlmeier, and O. T. Thomsen, "Development of a High-fidelity Experimental Substructure Test Rig for Grid-scored Sandwich Panels in Wind Turbine Blades," *Strain*, vol. 50, no. 2, pp. 111–131, apr 2014.

[13] L. Mishnaevsky, K. Branner, H. N. Petersen, J. Beauson, M. McGugan, and B. F. Sørensen, "Materials for wind turbine blades: An overview," *Materials*, vol. 10, no. 11, pp. 1–24, 2017.

[14] M. Rosemeier, M. Bätge, and A. Antoniou, "A novel single actuator test setup for combined loading of wind turbine rotor blade sub-components," in *2nd International Symposium on Multiscale Experimental Mechanics: Multiscale Fatigue*, 2017, pp. 1–10.

[15] F. Lahuerta, N. Koorn, and D. Smissaert, "Wind turbine blade trailing edge failure assessment with sub-component test on static and fatigue load conditions," *Composite Structures*, vol. 204, pp. 755–766, nov 2018.

[16] P. Hubert and a. Poursartip, "Aspects of the Compaction of Composite Angle Laminates: An Experimental Investigation," *Journal of Composite Materials*, vol. 35, no. 1, pp. 2–26, 2001.

[17] B. Hayman, C. Berggreen, and R. Pettersson, "The Effect of Face Sheet Wrinkle Defects on the Strength of FRP Sandwich Structures," *Journal of Sandwich Structures and Materials*, vol. 9, no. 4, pp. 377–404, 2007.

[18] M. Leong, L. C. T. Overgaard, O. T. Thomsen, E. Lund, and I. M. Daniel, "Investigation of failure mechanisms in GFRP sandwich structures with face sheet wrinkle defects used for wind turbine blades," *Composite Structures*, vol. 94, no. 2, pp. 768–778, 2012.

[19] M. Leong, C. F. Hvejsel, O. T. Thomsen, E. Lund, and I. M. Daniel, "Fatigue failure of sandwich beams with face sheet wrinkle defects," *Composites Science and Technology*, vol. 72, no. 13, pp. 1539–1547, 2012.

[20] T. J. Dodwell, R. Butler, and G. W. Hunt, "Out-of-plane ply wrinkling defects during consolidation over an external radius," *Composites Science and Technology*, vol. 105, pp. 151–159, 2014.

[21] S. Mukhopadhyay, M. I. Jones, and S. R. Hallett, "Tensile failure of laminates containing an embedded wrinkle; numerical and experimental study," *Composites Part A: Applied Science and Manufacturing*, vol. 77, pp. 219–228, 2015.

[22] J. W. Nelson, T. W. Riddle, and D. S. Cairns, "Effects of defects in composite wind turbine blades – Part 1: Characterization and mechanical testing," *Wind Energy Science Discussions*, vol. 2, pp. 641–652, apr 2017.

[23] L. D. Bloom, J. Wang, and K. D. Potter, "Damage progression and defect sensitivity: An experimental study of representative wrinkles in tension," *Composites Part B: Engineering*, vol. 45, no. 1, pp. 449–458, 2013.

[24] J. J. Bender, S. R. Hallett, and E. Lindgaard, "Parametric Study of The Effect of Wrinkle Features on The Strength of a Tapered Wind Turbine Blade Sub-structure," *Submitted to Composite Structures*, 2018.

[25] R. F. El-Hajjar and D. R. Petersen, "Gaussian function characterization of unnotched tension behavior in a carbon/epoxy composite containing localized fiber waviness," *Composite Structures*, vol. 93, no. 9, pp. 2400–2408, 2011.

[26] N. Xie, R. A. Smith, S. Mukhopadhyay, and S. R. Hallett, "A numerical study on the influence of composite wrinkle defect geometry on compressive strength," *Materials and Design*, vol. 140, pp. 7–20, 2018.